

## Deformation on isomeric excitation of Eu isotopes in $(\gamma, n)$ and $(n, \gamma)$ reactions

A. P. Tonchev,<sup>1,\*</sup> Yu. P. Gangrsky,<sup>2</sup> A. G. Belov,<sup>2</sup> and V. E. Zhuchko<sup>2</sup>

<sup>1</sup>*Department of Physics, Idaho State University, Pocatello, Idaho 83209*

<sup>2</sup>*Joint Institute for Nuclear Research, Dubna, 141980 Russia*

(Received 7 May 1998)

Isomeric ratios in  $(n, \gamma)$  and  $(\gamma, n)$  reactions in Eu isotopes were measured. Thermal neutrons and bremsstrahlung photons in the giant dipole resonance energy range of 13–22 MeV were used to excite the isomeric states. The isomeric levels  $0^-$  and  $8^-$  were excited in the isotopes  $^{150}\text{Eu}$ ,  $^{152}\text{Eu}$ , and  $^{154}\text{Eu}$ . The cross section for the reaction  $(\gamma, n)$  leading to the high-spin isomeric state  $8^-$  on  $^{152}\text{Eu}^{m2}$  isotope was measured in the giant-dipole-resonance region by the activation method. Experimental values of the isomeric cross section ratios were compared with the theoretical values. The influence of the nuclei quadrupole deformation on the isomeric ratio was described. [S0556-2813(98)03011-8]

PACS number(s): 25.70.Ef, 24.30.Cz, 27.70.+q

### I. INTRODUCTION

One of the main sources of information about the properties of excited states of nuclei is nuclear reactions involving various bombarding particles. These reactions allow the determination of several parameters of individual levels (spins, parities, electric and magnetic moments, matrix elements of radiative transition), and give information about the statistical properties of the levels at high excitation energies (the dependence of the level density on energy and angular momentum). When various bombarding particles are used, certain subsets of nuclear levels are selected and only some of these parameters are clearly manifested. Therefore, by using a wide range of particles to study nuclei, it is possible to obtain a complete picture of the properties of nuclear levels up to high excitation energies.

The large difference between the spins of a nucleus in isomeric and ground states is one of the reasons behind isomery; as a result, only radiative transitions of high multipole orders are possible in the deexcitation of an isomer. For deformed nuclei, there are also selection rules in the quantum number  $K$  (spin projection onto the symmetry axis of a nucleus) that lead to a large delay in radiative transitions of low multipole orders. A similar delay may be due to the difference in shape between an isomer and the corresponding ground-state nucleus. This is exemplified by spontaneously fissionable isomers, which are characterized by an anomalously large quadrupole-deformation parameter ( $\beta \approx 0.6$ ) and by a strong suppression of  $\gamma$  transitions to the ground state [1–3]. An additional delay for radiative transitions may be due to selection rules in the orbital angular momentum and in the isotopic spin, as well as to the fact that multiparticle configurations are very different.

Obviously, all factors that delay radiative transitions also manifest themselves in the probability of populating isomeric states through excited nuclear levels. However, the degree to which these factors are operative changes substantially with increasing excitation energy. For example, selection rules in

$K$  that are peculiar to deformed nuclei exert virtually no effect at excitation energies of a few MeV. The effect of nuclear deformation on the probability of exciting isomeric states has received much less study. The dependence of this probability on excitation energy has been measured only for a few spontaneously fissionable isomers ( $^{236}\text{U}$  and  $^{242}\text{Am}$ ). It was found that this probability increased sharply for excitation energies lower than the height of the potential barrier separating isomeric and ground states and that it reached a plateau at higher energies [2].

It was interesting to perform similar measurements for other nuclei where different deformations were realized for isomeric and ground states. Such cases are known in the regions between spherical and deformed nuclei. In  $N = 88$ –90 Sm and Eu isotopes, for example, different levels of the same residual nucleus could be excited in  $(d, t)$ ,  $(p, t)$ , and  $(t, p)$  reactions when spherical and deformed nuclei were used for targets [4–6]. This suggested that levels characterized by various values of the deformation parameters existed in these nuclei.

Here, experimental results for isomeric ratios (IRs)—the ratios of the cross sections (or yields) for reactions resulting in the production of nuclei in isomeric and ground states—were presented in reactions  $(\gamma, n)$  and  $(n, \gamma)$  on the spherical nucleus  $^{151}\text{Eu}$  and deformed nucleus  $^{153}\text{Eu}$  (Fig. 1). Evidence for the presence of this deformation was the evolution of the shape of a total photoneutron cross section in the giant dipole resonance region as the transition from spherical to statistically deformed nuclei was made. The photoneutron cross section for  $^{151}\text{Eu}$  had one peak, while  $^{153}\text{Eu}$  had two peaks, which was characteristic of deformed nuclei [7]. The isomers excited in these reactions had different values of the quadrupole-deformation parameter. Farther, the target nuclei had the same spin and parity ( $I^\pi = \frac{5}{2}^-$ ) and these reactions introduced small changes in angular momenta in the target ( $1\hbar$  and  $1/2\hbar$ , correspondingly) leading to small differences in the excitation of states built on these isomeric states. This measurement of IRs and comparison of these ratios for  $^{151}\text{Eu}$  and  $^{153}\text{Eu}$  targets furnished information about the effect of variations in deformation on the probability of isomer excitation.

\*Author to whom correspondence should be addressed.

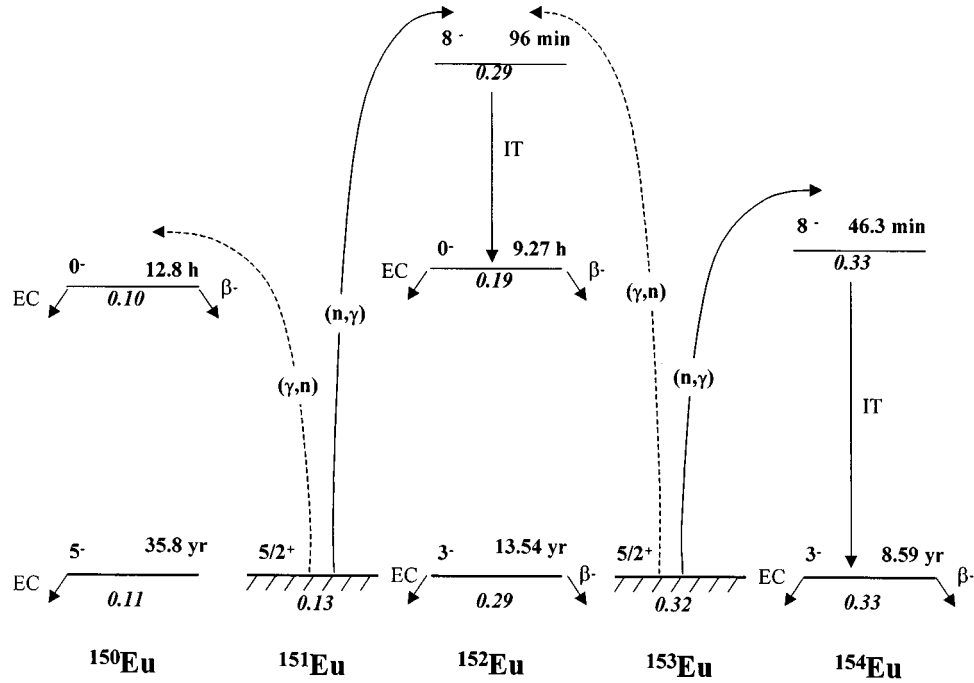


FIG. 1.  $(\gamma, n)$  and  $(n, \gamma)$  reactions on europium isotopes. Half-life, spin and parity, and quadrupole deformation (in italic) of each state are shown.

## II. SPECTROSCOPIC PROPERTIES OF Eu ISOTOPES

The spectroscopic features of the ground and isomeric states of  $^{150}\text{Eu}$ ,  $^{151}\text{Eu}$ ,  $^{152}\text{Eu}$ ,  $^{153}\text{Eu}$ , and  $^{154}\text{Eu}$  nuclei [8] are illustrated in Table I, which displayed their level energy,  $E_L$ ,  $\gamma$  radiation energy  $E_\gamma$ , intensity of the  $\gamma$  line, conversion coefficient  $\alpha$ , nucleon configurations, spectroscopic quadrupole moments  $Q_s$  [9], and the corresponding values of the deformation parameters  $\beta_2$ . The ground states of the odd-even nuclei were the  $d_{5/2}$  one-particle proton state for the spherical  $^{151}\text{Eu}$  nucleus and the  $[413]_{\frac{5}{2}}^5$  one-particle proton state for the deformed  $^{153}\text{Eu}$  nucleus. In the odd-odd nuclei,

the configurations of the ground  $3^-$  and isomeric  $8^-$  levels were determined by these proton states, and by the  $f_{5/2}$  neutron state for the spherical  $^{150}\text{Eu}$  nucleus and by the  $[505]_{\frac{1}{2}}^{11}$  neutron state for the deformed  $^{152}\text{Eu}$  and  $^{154}\text{Eu}$  nuclei. In addition, the  $0^-$  isomeric level in  $^{152}\text{Eu}$  had a different configuration: this level received contributions from the  $[411]_{\frac{3}{2}}^3$  proton state and the  $[532]_{\frac{3}{2}}^3$  neutron state, which were formed as the result of the splitting of the  $d_{3/2}$  and  $f_{7/2}$  one-particle states, respectively. That the ground and isomeric  $0^-$  levels in  $^{152}\text{Eu}$  have substantially different configurations was the reason why the radiative transition between them was strongly suppressed. This transition was not observed,

TABLE I. Spectroscopic features of ground and isomeric states of Eu isotopes.

| Isotope                | $E_L$<br>(keV) | $E_\gamma$<br>(keV) | $I_\gamma$<br>(%) | $\alpha$<br>(%) | Nucleon<br>configuration                             | $Q_s$<br>(b) | $\beta_2$ |
|------------------------|----------------|---------------------|-------------------|-----------------|--|--------------|-----------|
| $^{150}\text{Eu}^g$    | 0              | 334.0               | 94.0              | 3.2             | $p(d_{5/2}) + n(f_{5/2})$                            | 1.13(5)      | 0.11(1)   |
| $^{150}\text{Eu}^m$    | 42.1           | 349.4               | 78.68             | 1.2             | $p(d_{5/2}) - n(f_{5/2})$                            |              | (0.10)    |
|                        |                | 406.5               | 2.77              | 3.2             |  |              |           |
| $^{151}\text{Eu}^g$    | 0              | st.                 |                   |                 | $p(d_{5/2})$   | 0.903(10)    | 0.13(1)   |
| $^{152}\text{Eu}^g$    | 0              | 121.8               | 28.37             | 110             | $p[413]_{\frac{5}{2}}^5 - n[505]_{\frac{1}{2}}^{11}$ | 2.54(22)     | 0.29(3)   |
|                        |                | 964.1               | 14.63             | <1              |  |              |           |
| $^{152}\text{Eu}^{m1}$ | 45.6           | 121.8               | 7.2               | 110             | $p[411]_{\frac{3}{2}}^3 - n[532]_{\frac{3}{2}}^3$    |              | (0.19)    |
|                        |                | 841.6               | 14.59             | <1              |  |              |           |
| $^{152}\text{Eu}^{m2}$ | 147.8          | 89.8                | 72.36             | 34              | $p[413]_{\frac{5}{2}}^5 + n[505]_{\frac{1}{2}}^{11}$ |              | (0.29)    |
| $^{153}\text{Eu}^g$    | 0              | st.                 |                   |                 | $p[413]_{\frac{5}{2}}^5$                             | 2.412(21)    | 0.32(1)   |
| $^{154}\text{Eu}^g$    | 0              | 123.1               | 41.2              | 115             | $p[413]_{\frac{5}{2}}^5 - n[505]_{\frac{1}{2}}^{11}$ | 2.84(10)     | 0.33(2)   |
|                        |                | 1274                | 35.5              | <1              |  |              |           |
| $^{154}\text{Eu}^m$    | 160            | 68.2                | 37.2              | 0.7             | $p[413]_{\frac{5}{2}}^5 + n[505]_{\frac{1}{2}}^{11}$ |              | (0.33)    |
|                        |                | 100.9               | 25.3              |                 |  |              |           |

and a lower limit on the reduced probability of the  $M3$  transition was  $10^{-7}$  one-particle units.

In Table I the deformation-parameter values obtained from the spectroscopic quadrupole moments underwent a sudden change when going from  $^{151}\text{Eu}$  ( $N=88$ ) to  $^{152}\text{Eu}$  ( $N=89$ ). In the isomeric  $0^-$  state of  $^{152}\text{Eu}$ ,  $Q_s=0$ , did not allow the determination of the quadrupole-deformation parameter. However,  $\beta_2$  was estimated by using the isomeric shift of optical lines in the spectra of atoms or ions. This quantity was measured by resonance laser fluorescence [10]. The measured shift led to a difference of nuclear charge radii in the isomeric and ground states of  $\Delta\langle r^2 \rangle = 0.265(25) \text{ fm}^2$ . If the assumption that the volumes of nuclei in the ground and isomeric states are equal, this value of  $\Delta\langle r^2 \rangle$  corresponded to  $\Delta\beta_2 \cong 0.1$ , which yielded  $\beta_2 \cong 0.19$  for the  $^{152}\text{Eu}$  nucleus in the isomeric  $0^-$  state.

Thus, the ground and the isomeric  $0^-$  levels of the  $^{152}\text{Eu}$  nucleus were characterized by markedly different values of the quadrupole-deformation parameter. It is conceivable that these two levels were populated through different systems of excited states, in which case the isomeric ratio could be different for the spherical and deformed target nuclei in the reactions under study.

By analogy with the  $0^-$  level in  $^{152}\text{Eu}$ , it was assumed that the corresponding level in  $^{150}\text{Eu}$  was characterized by a small deformation (close to the ground-state deformation). At the same time, the isomeric  $I^\pi=8^-$  levels in  $^{152}\text{Eu}$  and  $^{154}\text{Eu}$  appeared to have a strong deformation, since they were formed from the same Nilsson proton and neutron configurations as the ground states. The estimates obtained in this way for the quadrupole-deformation parameters were also presented in Table I (in parentheses).

### III. EXPERIMENTAL PROCEDURE

The IRs in the  $(\gamma, n)$  and  $(n, \gamma)$  reactions in question were measured by using an electron beam extracted from the MT-25 microtron of the Flerov Laboratory of Nuclear Reactions at JINR, Dubna [11]. This electron beam was the source of both bremsstrahlung photons and neutrons. A cooled tungsten disk, 2-mm thick, served as a bremsstrahlung producing target. A 30-mm-thick aluminum absorber of electrons was arranged downstream of the disk. The energy of electrons was determined on the basis of the magnetic-field strength, measured by the NMR method, and the frequency of the accelerating electric field. The bremsstrahlung target was simultaneously employed for the collector of the electron current, which was measured by an electric-charge integrator.

To obtain neutrons, the electron beam was directed to a converter (uranium cylinder surrounded by beryllium). Beryllium also generated neutrons at the expense of the  $\gamma$  rays scattered by uranium and served as a neutron moderator. This uranium-beryllium converter was placed within a  $120 \times 120 \times 120 \text{ cm}^3$  graphite cube, which served as a main neutron moderator. The thermal-neutron flux at the center of the cube was  $4 \times 10^8 \text{ neutron}/(\text{s cm}^2)$  at an electron energy of 25 MeV and a current of  $20 \mu\text{A}$ .

Irradiated  $\text{Eu}_2\text{O}_3$  samples of natural isotopic composition or enriched in  $^{153}\text{Eu}$  had a weight of 100 mg and a surface area of  $1 \text{ cm}^2$ . Exposures to bremsstrahlung photons were

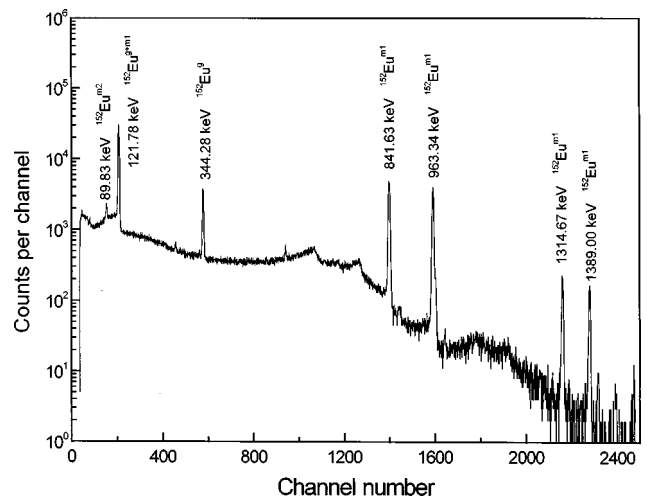


FIG. 2.  $\gamma$  spectrum obtained upon irradiating an enriched  $^{153}\text{Eu}$  (99.4%) target by bremsstrahlung with end-point energy  $E_{\gamma \text{ max}} = 15 \text{ MeV}$  (the exposure time was 1 h, the cooling time was 12 h, and the spectrum-acquisition time was 15 min).

performed for end-point energies in the range 13–22 MeV with an energy step of 1 MeV, the mean electron current being  $15 \mu\text{A}$ . An exposure time of 1 h ensured sufficient induced activity both for the ground and for the isomeric state. The half-lives of the radioactive nuclides under study were measured in a number of studies. Sample counting time was determined by the need for adequate statistics.

The same samples were also irradiated by neutrons for 1 h in the graphite cube at a distance of 40 cm from its center (at this point, the cadmium ratio was 2.5). To take into account the contribution of resonance neutrons to the yield of Eu isotopes, similar exposures were performed with samples shielded by a 2-mm-thick cadmium foil. Eu isotopes originating from the  $(\gamma, n)$  and  $(n, \gamma)$  reactions in the ground and isomeric states were identified by their  $\gamma$  radiation and by their half-lives (the features of the radioactive decay of Eu isotopes were presented in Fig. 1 and Table 1 from Ref. [8]). The  $\gamma$  spectra of the samples subjected to irradiation were measured by using a Ge(Li) detector with a fiducial volume of  $60 \text{ cm}^3$ . The energy resolution of this detector was 3 keV for the 1332-keV  $\gamma$  line of  $^{60}\text{Co}$ . Figure 2 illustrates one such spectrum displaying the  $\gamma$  lines presented in Table I. The spectra were processed with the ACTIV code [12], which permitted the separation of  $\gamma$  lines with close energies in complicated spectra.

### IV. EXPERIMENTAL RESULTS

Some preliminary experimental results of these measurements were described in Ref. [13]. Here the results were compared with theoretical calculations from other publications.

The measured intensities of  $\gamma$  lines made it possible to determine the absolute yields of Eu nuclei in the ground and isomeric states from the above photon- and neutron-induced reactions and the isomeric ratios as functions of the end-point energy of the bremsstrahlung spectrum or of nuclear-excitation energy. By the IR in the  $(\gamma, n)$  reaction, the ratio of the yields for a given end-point energy of the bremsstrahlung spectrum is meant. For  $(n, \gamma)$  reactions, this quantity

was defined as the ratio of the cross sections. The relation between the areas under the  $\gamma$  peaks corresponding to the isomeric and ground states ( $S_m$  and  $S_g$ , respectively) and the IR were determined by the equation

$$\text{IR} = \frac{Y_m}{Y_g} = \left[ \frac{\lambda_g f_m(t)}{\lambda_g f_m(t)} \left( \frac{S_g \varepsilon_m I_m (1 + \alpha_g)}{S_g \varepsilon_m I_m (1 + \alpha_m)} - p \frac{\lambda_g}{\lambda_g - \lambda_m} \right) + p \frac{\lambda_m}{\lambda_g - \lambda_m} \right]^{-1}, \quad (1)$$

where the indices  $m$  and  $g$  refer to the isomeric and ground states, respectively,  $\varepsilon$  is the detection efficiency for the  $\gamma$  line being investigated,  $I$  is its intensity,  $\alpha$  is the conversion ratio,  $\lambda$  is the decay constant, and  $p$  is the probability of the transition from the isomeric to the ground state. The time-dependent factor  $f(t)$  that took into account the accumulation and decay of nuclei was given by

$$f(t) = (1 - e^{-\lambda t_i}) e^{-\lambda t_c} (1 - e^{-\lambda t_m}), \quad (2)$$

where  $t_i$ ,  $t_c$ ,  $t_m$  were the times of irradiation, decay, and measurement. Because the isomeric and ground states were obtained in the same exposure run and because the required quantities (yields or cross sections) were measured for them under identical conditions, the errors associated with the intensities of bremsstrahlung and neutron fluxes and with the geometry of exposures and measurements were eliminated in determining IRs.

The following difficulties had to be circumvented in measuring the IRs in the reactions leading to the production of Eu isotopes.

(i) The half-lives of Eu nuclei in the ground and isomeric states differed dramatically (by a factor exceeding 1000). For this reason, the intensities of  $\gamma$  radiation emitted by them also greatly differed, so that measurements for an isomer and for a ground-state nucleus had to be performed either under different geometric conditions or in different time intervals. In addition, large corrections for isomer decay had to be introduced.

(ii) The spectrum of  $\gamma$  radiation emitted by a mixture of Eu isotopes and isomers was very intricate: there were several tens of  $\gamma$  lines in all, and some of them belonged both to the ground and to isomeric states. In view of this, it was necessary to perform a thorough analysis of the spectrum and the intensities of the  $\gamma$  lines under study as functions of time.

(iii) The cross sections for the reactions  $^{151}\text{Eu}(n, \gamma)$  that were induced by thermal neutrons and which led to the production of the Eu ground  $I^\pi = 3^-$  and isomeric  $I^\pi = 0^-$  states were large (6000 and 3150 b, respectively [14]). When the IRs for  $(\gamma, n)$  reactions were measured, the contribution of thermal neutrons formed owing to the deceleration of neutrons from the bremsstrahlung target had to be correctly taken into account. For this reason, the Eu samples were exposed to bremsstrahlung under conditions that reduced the thermal-neutron flux at the point of irradiation to the maximum possible degree. All the materials that moderated neutrons (floor, walls, and absorber of  $\gamma$  radiation) were at a distance greater than 1 m. The contribution to the yield of  $^{152}\text{Eu}^m$  and  $^{152}\text{Eu}^g$  from thermal neutrons was determined from the yield of the  $^{52}\text{V}$  isotope ( $T_{1/2} = 3.7$  min) produced

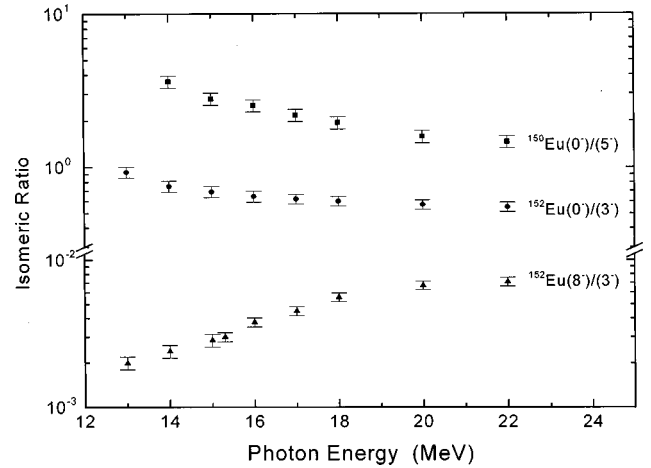


FIG. 3. The yield ratio dependence in  $(\gamma, n)$  reactions on Eu isotopes vs the maximum energy of the bremsstrahlung radiation.

in the reaction  $^{51}\text{V}(n, \gamma)$  at the maximum electron energy of 22 MeV. It was found to be less than 10%.

The measured IRs of the yields from  $\gamma, n$  reactions are presented in Fig. 3 as functions of the end-point energy of the bremsstrahlung spectrum. The error in the absolute values of the IRs was 10%. The contributions to this error came from the statistics of events in the  $\gamma$  peaks, from the uncertainties in the detection efficiency for photons and in the intensity of the chosen  $\gamma$  transition in the decay diagram. In the relative IR values, which determined the shape of the dependences of IRs on the excitation energy (Fig. 3) or were used for comparison with the IRs in the reactions  $(n, \gamma)$ , the last two uncertainties were eliminated, and the error in the IRs was reduced to 2%.

It can be seen from Fig. 3 that, for  $0^-$  levels, the IR decreased with increasing energy of  $\gamma$  radiation, but that it grew for  $8^-$  levels. The last correspondence agreed with that obtained in Ref. [15]. In contrast, the  $Y(8^-)/Y(3^-)$  ratio increased strongly with increasing excitation. This change was more perceptible in the beginning of the curve. The observed behavior of the IRs corresponded to the known regularities in their variations with increasing excitation energy and angular momentum of the nucleus under study.

The yield of  $^{152}\text{Eu}^{m2}$  isomeric state as a function of the bremsstrahlung endpoint energy was obtained from the measurements of the ratios of the yields for the isomeric states and for the monitoring reaction. These dependences were input data for the determining partial cross sections for the photonuclear reactions. One method that permitted the study of cross sections for photonuclear reactions as a functions of the excitation energy and nucleonic composition of nuclei employed the relative method of measurement. Here, measured quantities are normalized to a well-known cross section taken as a reference. As in Ref. [16], the cross section for the reaction  $^{65}\text{Cu}(\gamma, n)^{64}\text{Cu}$  [17] was taken for the reference. An enriched (99.4%)  $^{153}\text{Eu}$  isotope was used as the target material. To reconstruct the reaction cross section, an interactive procedure for minimizing directed divergences was employed [18]. The step used in reconstructing the cross section was 1 MeV. Figure 4 displays the excitation function for the reaction  $(\gamma, n)$  leading to the  $^{152}\text{Eu}^{m2}$  high spin isomeric state. The same figure also shows the total photo-

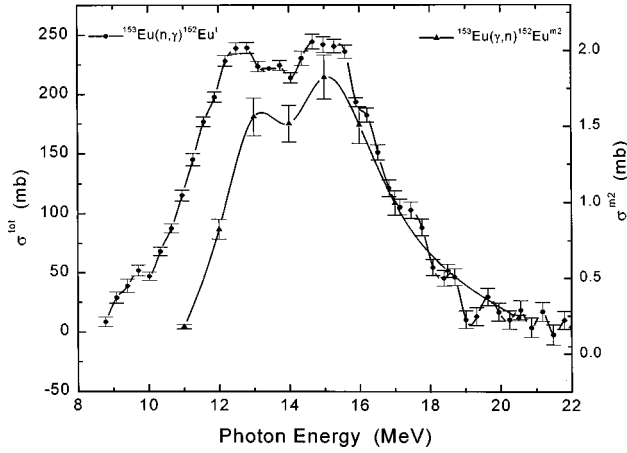


FIG. 4. Excitation function of the reaction  $^{153}\text{Eu}(n, \gamma)\text{Eu}^{\text{tot}}$  (●) and  $^{153}\text{Eu}(\gamma, n)\text{Eu}^{\text{m}2}$  (▲) in energy diapason from threshold to the 22 MeV. The curve is a spline curve fitted to the cross section data. Photoneutron cross section for the  $(\gamma, n)^{\text{tot}}$  was taken from Ref. [7].

neutron cross section on the  $^{153}\text{Eu}$  leading to the ground state [7].

The IR measured for the  $I^\pi=0^-$  isomer from the reaction  $^{151}\text{Eu}(n, \gamma)^{152}\text{Eu}$  amounted to 0.52 (1) for thermal neutrons. This IR lay within known values ranging from 0.43 [19] to 0.65 [20]. The spread in these IR values can to be explained by uncertainties in the intensities of the measured  $\gamma$  lines (different in each experiment) and by variations in the contribution to the observed yield from resonance neutrons. For the  $I^\pi=8^-$  isomers from the reactions  $^{151}\text{Eu}(n, \gamma)$  and  $^{153}\text{Eu}(n, \gamma)$ , more estimates of the IRs,  $7 \times 10^{-4}$  for  $^{153}\text{Eu}$  and  $3 \times 10^{-4}$  for  $^{154}\text{Eu}$ , were unobtainable because the yields of these isomers were very low and because the background of  $\gamma$  radiation emitted in the decay of the  $^{152}\text{Eu}$  isomer ( $I^\pi=0^-$ ) was intense. These estimates were in accord with the known values from Refs. [14,21]

V. DISCUSSION

All six reactions investigated here were divided into three groups according to the change undergone by the quadrupole

deformation as the initial target nucleus ( $^{151}\text{Eu}$  or  $^{153}\text{Eu}$ ) was transformed into a final nucleus produced in the ground or in one of the isomeric states (with  $I^\pi=0^-$  or  $8^-$ ).

(i) The deformation changed when the nucleus was produced in an isomeric state, but it remained unchanged in the ground state. This case was exemplified by the reaction  $^{153}\text{Eu}(\gamma, n)^{152}\text{Eu}^{\text{m}}$  ( $I^\pi=0^-$ ).

(ii) The opposite case was that the deformation did not change when the nucleus was produced in an isomeric state, but it changed when the nucleus was produced in the ground state, as occurred in the reaction  $^{151}\text{Eu}(n, \gamma)^{152}\text{Eu}(I^\pi=0^-)$ .

(iii) In the production of a nucleus both in the ground and in the isomeric states, the deformation either underwent no change or change identical for the two states. This group included the reactions resulting in the production of  $^{152}\text{Eu}$  and  $^{154}\text{Eu}$  in isomeric  $I^\pi=0^-$  state because the deformation of the nucleus in these states was identical to that in the ground state.

If the change in nuclear deformation affected the probability of isomer excitation, as is the case of spontaneously fissile isomers (see above), a reduction of this probability could be expected for the reaction from the first group. At the same time, the probability of nucleus production in the ground state would decrease for the reactions from the second group. As the result, the IRs for the reactions from the third group would be greater than the IRs for the reactions from the first group and less than the IRs for reactions from the second group.

Table II displays the IRs for all reactions investigated here; the groups to which these reactions belong are also indicated. In comparison, the results from Refs. [14,15,19–22] are also presented. No expected dependence of the IRs on the group of reactions was observed. For example, it was noted for the  $I^\pi=0^-$  isomer of  $^{152}\text{Eu}$ , the deformation changed in the reaction  $(\gamma, n)$  but not in the reaction  $(n, \gamma)$ . The situation was reversed for the  $^{152}\text{Eu}$  ground state. However, instead of an IR value that was smaller in the  $(\gamma, n)$  reaction than in the  $(n, \gamma)$  reaction, the

TABLE II. Isomeric ratios in  $(\gamma, n)$  and  $(n, \gamma)$  reactions.

| Reactions                                   | $I_m^\pi$ | Group     | $E^*$<br>(MeV) | IR             | Calculation |
|---|-----------|-----------|----------------|----------------|-------------|
| $^{151}\text{Eu}(\gamma, n)^{150}\text{Eu}$ | 0-        | 3         | 3.5            | 2.10(5)        |             |
|   |           |           | 5.0            | 1.53(3)        | 0.65        |
| $^{151}\text{Eu}(n, \gamma)^{152}\text{Eu}$ | 0-        | 2         | 6.31           | 0.52(1)        | 0.19        |
|   |           |           |                | 0.53(2) [12]   | 0.47 [15]   |
|   |           |           |                | 0.43(6) [14]   | 0.12 [24]   |
|   |           |           |                | 0.65(1) [15]   | 0.11 [25]   |
|   |           |           |                | 0.54(2) [17]   |             |
| $^{153}\text{Eu}(\gamma, n)^{152}\text{Eu}$ | 8-        | 3         | 6.31           | 0.0007(2)      | 0.0015      |
|   |           |           | 0-             | 1              | 2.5         |
|   | 8-        | 3         | 2.5            | 0.57(1)        | 0.20        |
|   |           |           |                | 0.0029(1)      |             |
|   |           |           |                | 0.0040(4) [13] |             |
|   | 4.0       | 0.0071(2) | 0.025          |                |             |
| $^{153}\text{Eu}(n, \gamma)^{154}\text{Eu}$ | 8-        | 3         | 6.44           | 0.00031(3)     |             |

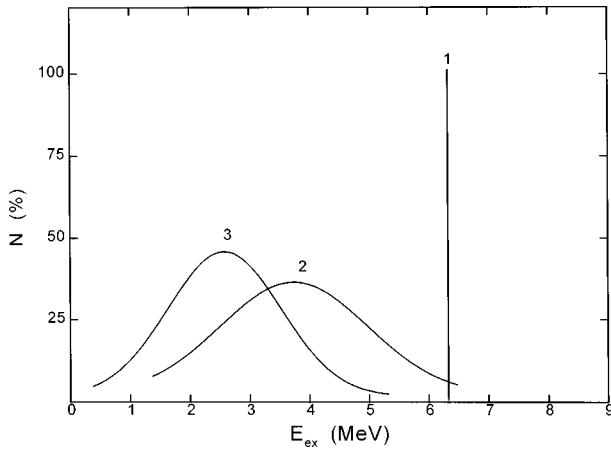


FIG. 5. Excitation-energy distribution of  $^{152}\text{Eu}$  nuclei (1) in the  $(n, \gamma)$  reaction upon neutron capture and (2 and 3) in the  $(\gamma, n)$  reaction upon neutron emission at bremsstrahlung end-point energies of 22 and 15 MeV, respectively.

opposite was observed. For reactions in which the final nuclei in isomeric and ground states had close values of the deformation parameter (reaction leading to the production of an  $I^\pi = 8^-$  isomer), nearly equal values of the IRs were expected. However, the IR values were markedly different for different reactions and for different final nuclei (see Fig. 1).

To some extent, the observed variations in the IR values can be associated with distinctions between the excitation-energy and angular-momentum distributions of the final nucleus prior to the photon cascade populating the isomeric and ground states. These distributions, were formed upon neutron capture in  $(n, \gamma)$  reactions. As to  $(\gamma, n)$  reactions, the formation of the excitation-energy and angular-momentum distributions occurred following neutron emission from an excited nucleus produced as the result of photon absorption. In the latter case, the energy distribution was comparatively broad because of the bremsstrahlung spectrum of  $\gamma$  radiation. For instance, Fig. 5 showed the distribution of excitation energy of residual nuclei for the reaction  $^{153}\text{Eu}(\gamma, n)^{152}\text{Eu}$ , assuming that the endpoint energy of the bremsstrahlung spectrum was 22 and 15 MeV. The mean value of this distribution was determined by the equation

$$E^* = E_{\text{eff}} - B_n - \varepsilon_n, \quad (3)$$

where  $E_{\text{eff}}$  is the effective excitation energy,  $B_n$  is the neutron binding energy, and  $\varepsilon_n$  is the kinetic energy of the neutron escaping from the nucleus. A peculiarity of photonuclear reactions with the bremsstrahlung lay in the fact that in the process of photoexcitation, the  $\gamma$  quanta both with the minimum energy and with the energy equal the maximum electron energy were involved. Thus the energy center of gravity was determined by the ratio

$$E_{\text{eff}} = \frac{\int_{E_{\text{th}}}^{E_{\gamma\text{max}}} E \sigma(E) N(E, E_{\gamma\text{max}}) dE}{\int_{E_{\text{th}}}^{E_{\gamma\text{max}}} \sigma(E) N(E, E_{\gamma\text{max}}) dE}, \quad (4)$$

where  $\sigma(E)$  is the cross section for the absorption of a photon with energy  $E$  by a nucleus and  $N(E, E_{\gamma\text{max}})$  is the number of photons with energy  $E$  in the bremsstrahlung spec-

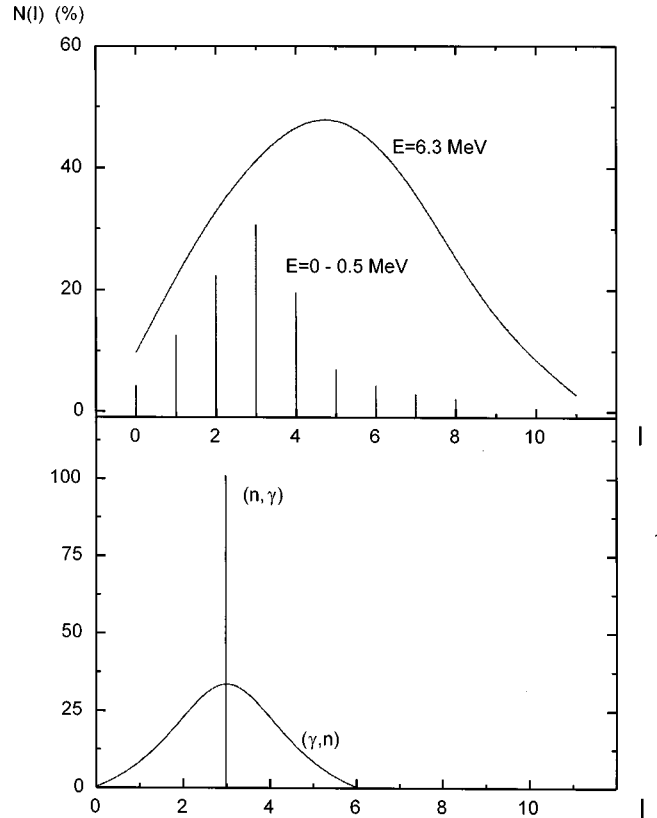


FIG. 6. Angular-momentum distribution of  $^{152}\text{Eu}$  nuclei. The lower plot shows the results for the  $(n, \gamma)$  and  $(\gamma, n)$  reaction at the excitation energies indicated in Fig. 4. The upper plot presents distributions obtained on the basis of (solid curve) the statistical model and (vertical bars) the known energy-level diagram (the excitation energy is indicated for each distribution).

trum. In these calculations, the known excitation functions for the photonuclear reactions featuring  $^{151}\text{Eu}$  and  $^{153}\text{Eu}$  [7] were employed. The experimental kinetic energy spectra of neutrons with a mean energy of 1 MeV [23] and the bremsstrahlung spectra used in the experiments were reported here [24].

The angular-momentum distribution of nuclei following neutron emission in the  $(\gamma, n)$  reaction was calculated by using the optical potential for neutron-nucleus interaction [25] and the parameters that described the statistical properties of levels in Eu isotopes [26]. For the above reaction and under the same conditions, the distribution is presented in Fig. 6.

From the comparison of these distributions for the two reactions, the mean angular momentum of an excited nucleus in the  $(\gamma, n)$  reaction was equal to the nuclear spin after neutron capture ( $I=3$ ), the corresponding distribution being comparatively broad (the half-width is  $\Delta I \sim 3$ ). At the same time, the mean excitation energy was markedly lower even at the highest end-point energy of the bremsstrahlung spectrum (the values of the angular momentum and excitation energies are presented in Table II).

To assess the effect of these distributions on the IRs, these ratios were calculated on the basis of the statistical model by using the EMPIRE code [27] with parameters describing the level density as a function of energy and angular momentum for excitation energies higher than 1 MeV ( $a = 21 \text{ MeV}^{-1}$

and  $\sigma=4.8$  [26]). In the region  $E < 1$  MeV, the energy-level diagram known from the photon spectra measured following neutron capture was used [19,21]. For  $^{152}\text{Eu}$  nuclei, the two angular-momentum distributions of levels are presented in Fig. 6. The IRs calculated in this way and results of similar calculations from [28–30] are presented in Table II.

Comparison of the experimental and calculated IRs showed that for the two reactions and for the above parameter values, the calculation correctly reproduced the dependence of the IRs on the excitation energy. However, it led to the underestimated IR values for the  $I^\pi=0^-$  isomer and to the overestimated values for the  $I^\pi=8^-$  isomer. The same feature of the IR for the  $0^-$  isomer in  $^{152}\text{Eu}$  excited in the  $(n, \gamma)$  reaction was also noted in Refs. [28,29]. In all probability, the experimental values of the IRs could be explained by an excitation energy. In Fig. 6, as the excitation energy decreased, the spin distribution was shifted toward lower values. Moreover, an investigation of the reaction  $^{180}\text{Ta}^m(\gamma, \gamma')^{180}\text{Ta}^g$  in Ref. [30] revealed that a considerable contribution to the population of the low-spin isomers came from the levels of the rotational band built on the isomer state.

The calculations for the  $0^-$  isomer in  $^{152}\text{Eu}$  also demonstrated that the lower excitation energy and the broader spin distribution in the  $(\gamma, n)$  reaction in relation to the IR value were insignificant (from 0.19 to 0.22). At the same time, for the  $8^-$  isomer in  $^{152}\text{Eu}$ , the broader angular-momentum

spectrum in the  $(\gamma, n)$  reaction led to a sizable growth of the IR and this conclusion was confirmed by experimental data.

The different behavior in Fig. 3 could be explained by statistical theory. For example, IRs of high to the low spin increased with increasing excitation energy. In contrast, for low spin to high spins, IR decreased with increasing excitation energy. More activation levels with high spin were excited in the last case when incident energy increased. For example, 15 to 22 MeV coincided to both 2.4 and 3.7 MeV mean excitation energy after one neutron emission. This led to the increased high spin yield and, as a consequence, decreased IR.

Thus, this investigation showed that for the Eu isotopes, deformation affected slightly the probability of isomer population in  $(\gamma, n)$  and  $(n, \gamma)$  reactions. In contrast to spontaneously fissile isomers, the change undergone here by the deformation as the initial nucleus transitions into the final-state nucleus was overly small ( $\Delta\beta \sim 0.1$ ) to result in a strong suppression of radioactive transitions between levels characterized by different nuclear deformations.

### ACKNOWLEDGMENTS

The authors express their gratitude to H. G. Hristov for his assistance and technical support with the experiment and to N. P. Balabanov and J. F. Harmon for their invaluable comments.

---

[1] S. M. Polikanov, *Isomeric Nuclear Shapes* (Atomizdat, Moscow, 1977).

[2] Yu. P. Gangrsky, *Fiz. Elem. Chastits At. Yadra* **9**, 383 (1978).

[3] Yu. P. Gangrsky, A. P. Tonchev, and N. P. Balabanov, *Phys. Part. Nuclei* **27**, 428 (1996).

[4] J. H. Bjerregard, O. Hansen, O. Nathan, and S. Hidns, *Nucl. Phys.* **86**, 145 (1966).

[5] P. Debenham and N. H. Hintz, *Nucl. Phys.* **A195**, 865 (1972).

[6] G. Struble, I. Oelrich, and J. Carlson, *Phys. Rev. Lett.* **39**, 533 (1977).

[7] T. J. Boal, E. G. Muirhead, and D. J. S. Findlay, *Nucl. Phys.* **A406**, 257 (1983).

[8] *Tables of Isotopes*, edited by R. B. Firestone (Wiley, New York, 1996).

[9] P. Raghavan, *At. Data Nucl. Data Tables* **42**, 189 (1989).

[10] G. D. Alkhozov *et al.*, *Z. Phys. A* **316**, 123 (1984).

[11] A. G. Belov, *Workshop on the Application of Microtrons in Nuclear Physics*, Plovdiv, Bulgaria, 1992, Dubna JINR, 1993, Report No. D15-93-80, p. 12.

[12] V. I. Zlokazov, *Comput. Phys. Commun.* **28**, 27 (1982).

[13] A. G. Belov, Yu. P. Gangrsky, A. P. Tonchev, and V. E. Zhuchko, *Phys. At. Nucl.* **60**, 1773 (1997).

[14] S. F. Mughabghab, *Neutron Cross Sections* (Academic, New York, 1984), Vol. 1, Pt.B.

[15] I. N. Vishnevskii, V. A. Zheltonozhski, V. M. Mazur, and Z. M. Bigan, *Vopr. At. Nauki Tekh., Ser.: Yad. Konstanty* **61**, 21 (1991).

[16] A. G. Belov, Yu. P. Gangrsky, A. P. Tonchev, N. P. Balabanov, and H. G. Hristov, *Phys. At. Nucl.* **59**, 367 (1996).

[17] S. S. Dietrich and B. L. Berman, *At. Data Nucl. Data Tables* **38**, 199 (1988).

[18] V. E. Zhuchko, *Sov. J. Nucl. Phys.* **25**, 124 (1977).

[19] T. Von Egidy *et al.*, *Z. Phys. A* **286**, 341 (1978).

[20] V. F. Pshenichnui and E. A. Gritsai, *Yad. Fiz.* **51**, 621 (1990).

[21] W. H. Zoller, W. R. Walters, P. W. Gallagher, and R. A. Meger, *Phys. Rev. C* **13**, 2024 (1976).

[22] I. Poortam, I. Girlea, and A. Fabry, *Nucl. Phys.* **A172**, 489 (1971).

[23] A. M. Goryachev and G. N. Zalesnyi, *Izv. Akad. Nauk SSSR, Ser. Fiz.* **54**, 2240 (1990).

[24] Ph. G. Kondev, A. P. Tonchev, Kh. G. Khristov, and V. E. Zhuchko, *Nucl. Instrum. Methods Phys. Res. B* **71**, 126 (1992).

[25] C. M. Perey and F. G. Perey, *At. Data Nucl. Data Tables* **17**, 2 (1976).

[26] Yu. V. Sokolov, *Plotnost' urovnei atomnykh yader* (Nuclear Level Densities) (Energoatomizdat, Moscow, 1990).

[27] M. Herman, A. Marcinkovski, and K. Stankiewicz, *Comput. Phys. Commun.* **33**, 373 (1984).

[28] L. Ya. Arifov, B. S. Mazitov, and V. G. Ulanov, *Yad. Fiz.* **34**, 1028 (1981).

[29] W. P. Pointz, *Z. Phys.* **197**, 262 (1966).

[30] A. G. Belov, Yu. P. Gangrsky, A. P. Tonchev, and P. Zuzaan, *Hyperfine Interact.* **107**, 167 (1997).